THREE-DIMENSIONAL PHASE-FIELD SIMULATIONS OF EUTECTIC SOLIDIFICATION AND COMPARISON TO *IN SITU* EXPERIMENTAL OBSERVATIONS

Andrea Parisi[1], Mathis Plapp[1], Silvère Akamatsu[2], Sabine Bottin-Rousseau[2], Mikaël Perrut[2], and Gabriel Faivre[2]

[1] Laboratoire de Physique de la Matière Condensée, CNRS UMR 7643, Ecole Polytechnique, 91128 Palaiseau, France
[2] Institut des Nanosciences de Paris, CNRS UMR 7588, Université Pierre-et-Marie-Curie, Campus Boucicaut, 140 rue de Lourmel, 75015 Paris, France

Keywords: Phase-field simulation, solidification, eutectic alloys, morphological stability

The phase-field method has become the method of choice for simulating microstructure formation during solidification. Recent progress, both on the formulation of the model and on the numerical implementation, makes it now possible to simulate quantitatively the evolution of complex microstructures in three dimensions. This is illustrated by simulations of eutectic coupled growth. The morphological stability of lamellar patterns is investigated, and the results are compared to experimental data obtained by *in situ* observations of the transparent alloy carbontetrabromide-hexachloroethane. When the lamellar spacing exceeds a critical value, a zigzag instability occurs. The further evolution of the system leads to stable zigzag structures or lamella breakup, depending on the parameters.

Introduction

Recent years have seen rapid progress in the technique of phase-field modeling. While for a long time the simulations could only yield qualitative answers to questions of microstructure selection and morphological stability of solidification patterns, an ever increasing number of situations can be modeled quantitatively. The dendritic solidification of a pure substance has been simulated both at high and low undercoolings using the symmetric model of solidification [1, 2]. More recently, alloy solidification has been treated in free and directional growth using the one-sided model, both for single-phase and two-phase solidification [3, 4]. Models including fluid flow [5] or simultaneous heat and solute diffusion [6] have also been developed.

The maximum benefit of this progress can be reaped by a critical comparison of simulations and experiments. On the one hand, the capability of the model to reproduce experimental observations constitutes a validation of the hypotheses and simplifications inherent to any mathematical model. On the other hand, the simulations can yield insights into the physical mechanisms involved that are very difficult to extract from experiments.

This is illustrated here by experiments and simulations of eutectic solidification. When alloys with overall composition close to the eutectic composition are solidified, two-phase composite microstructures typically arise, with a lamellar or fibrous microstructure. Since the seminal work of Jackson and Hunt [7] it is known that there exist families of steady-state solutions for lamellae and rods, parametrized by the spacing between microstructural units. While Jackson and Hunt postulated that the state corresponding to a minimum front undercooling should be selected, subsequent work, both experimental [8] and numerical [9],

has shown that in thin samples (quasi-two-dimensional geometry) a whole range of spacings is stable. Thus, the final spacing depends on the initial conditions and the growth history. The range of stable spacings is limited on both sides by dynamic instabilities. For low spacings, a long-wavelength lamella elimination instability occurs; for large spacings, various short-wavelength oscillatory instabilities appear.

Here, we show that in massive samples (full three-dimensional geometry), the first instability to occur for large spacings is a zigzag instability, absent in two dimensions. This instability is observed both in experiments and simulations, albeit with a somewhat different critical spacing. The simulations allow us to identify all possible instabilities, to clarify their connection with the well-known two-dimensional instabilities, and to map out the complete stability diagram in the spacing-composition plane.

The remainder of the paper is organized as follows: first, the experimental setup is described, and the main experimental results are presented. Next, the phase-field model and simulation setup are briefly described. Finally, some simulation results will be described and related to the experimental findings.

Experimental Method

The experiments consisted in real-time observations of directional-solidification fronts of a transparent non-faceted eutectic in thin and massive samples. The transparent alloy is introduced in a glass crucible, placed in an external unidirectional gradient G, and pulled at a constant rate V through the gradient. The growth front is observed *in situ* with an optical microscope. We used a nearly eutectic CBr_4-C_2Cl_6 alloy. This alloy has a eutectic plateau at 84.4°C bordered by two solid solutions α and β of cubic (f.c.c and b.c.c., respectively) crystal structures, both growing from the melt in a fully non-faceted way. The relevant material constants of this alloy are known, in particular, the interlamellar spacing $\lambda_{\min}$ for which the front undercooling is minimum [7]. Near the eutectic composition, $\lambda_{\min} \approx 14.2\mu$m at $V = 1\mu\text{ms}^{-1}$ [10]. It is known that $\lambda_{\min}$ scales as $V^{-1/2}$ [7], and that all morphological transitions occur at critical spacings which are proportional to $\lambda_{\min}$ [9]. Therefore, in the following, all lamellar spacings λ will be expressed in dimensionless form as $\Lambda = \lambda/\lambda_{\min}$.

We used either 12 μm-thick ("thin") or about 400 μm-thick ("thick") parallelepiped-shaped glass crucibles. To avoid perturbations due to eutectic grain boundaries and surface tension anisotropy, we grow weakly anisotropic single eutectic grains containing several hundreds of lamella pairs. In thin samples, the lamellae are forced to remain perpendicular to the sample plane by the wall effects (no flux condition), but can rotate about the normal to this plane. The dynamics of the system is thus essentially two-dimensional. The front is reduced to a mere line, and can be observed in side view with a conventional optical microscope. The evolution of the shape of the front can be followed in real time with an accuracy of about 0.1μm. This configuration has been used extensively for years, which permitted an accurate quantitative determination of the 2D morphology diagram of CBr_4-C_2Cl_6 [8, 9, 10].

In bulk samples, eutectic lamellae are not aligned normal to the sample walls – at least not instantaneously – contrary to what occurs in thin samples. It is thus necessary to observe the growth front from the top through the liquid. Frontal (parallel to the growth axis) observation is excluded since it would deliver superposed images of the front itself and the underlying two-phase microstructure. We have built a new instrument [11], in which this problem is solved as follows. We observe the growth front in oblique view through a wall of the crucible. The direction of lighting is also oblique, but different from the direction of observation. The contrast between α and β originates from the difference of refraction angle of the light beams emerging from different phases (Fig. 1). By using a long-distance microscope (Questar QM100), and judiciously choosing the directions of observation and

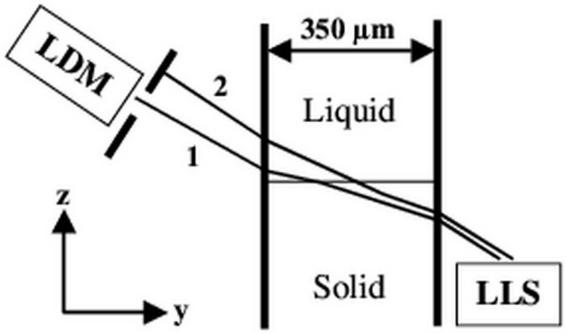

Figure 1: Sketch of the method of observation in thick samples. z is the axis of the thermal gradient . The sample is pulled in the $-z$ direction. y is normal to the glass wall of the crucible, through which the observation is made. LDM: long-distance microscope. LLS: linear light source. Rays 1 and 2 run through a β and a α lamella, respectively. The reduction of the image in the y direction due to the oblique direction of observation is corrected numerically.

lighting, one can make one of the phases appear bright, the other dark in the micrographs. The spatial resolution of this method is of the order of 1 μm, and the depth of field is of about 200 μm.

Experimental Results

We have performed long (>2h) solidification runs in a series of 350 μm-thick samples of CBr_4-C_2Cl_6 for various values of V in the range 0.1-1 μms^{-1}. Each run began by a short ($\approx$ 5 min) initial transient corresponding to the emergence of coupled growth by an invasion process [12]. This process occurs very rapidly so that its details are not directly observable by our methods. Both the average spacing and the arrangement of the pattern at the end of the invasion varied from sample to sample. Some samples exhibited a highly disordered pattern characterized by a multitude of small lamellar domains separated by regions containing a high density of topological defects (Fig. 2a). No preferred orientation of the lamellae was visible, except near the sides of the sample, where the lamellae were normal to the crucible wall. Such patterns remain disordered until the end of the experiment. In the other samples, the initial pattern exhibited a preferential orientation of the lamellae normal to the glass plates, and most of the topological defects present are progressively eliminated during further solidification (Fig. 2b). The few lamella terminations which survived in the final steady state are probably produced by perturbations such as grain boundaries or a lateral bias in the thermal field.

In a few samples, the final stationary pattern exhibited an in-phase sinusoidal deformation of the lamellae (Fig. 2c) [11]. Such "zigzag" patterns – and the corresponding zigzag bifurcation – are well known in other pattern-forming dynamical systems such as Rayleigh-Bénard convection [13]. In our case, the appearance of zigzag patterns in some experiments was clearly correlated with the fact that the scaled average spacing Λ was larger in those than in the other experiments. This indicates that the lamellar pattern undergoes a zigzag bifurcation above some critical spacing Λ_{zz}. We measured the values of the amplitude A of the zigzags as a function of Λ (i.e. of V and λ) and found the bifurcation threshold at $\Lambda_{zz} \approx 0.85$.

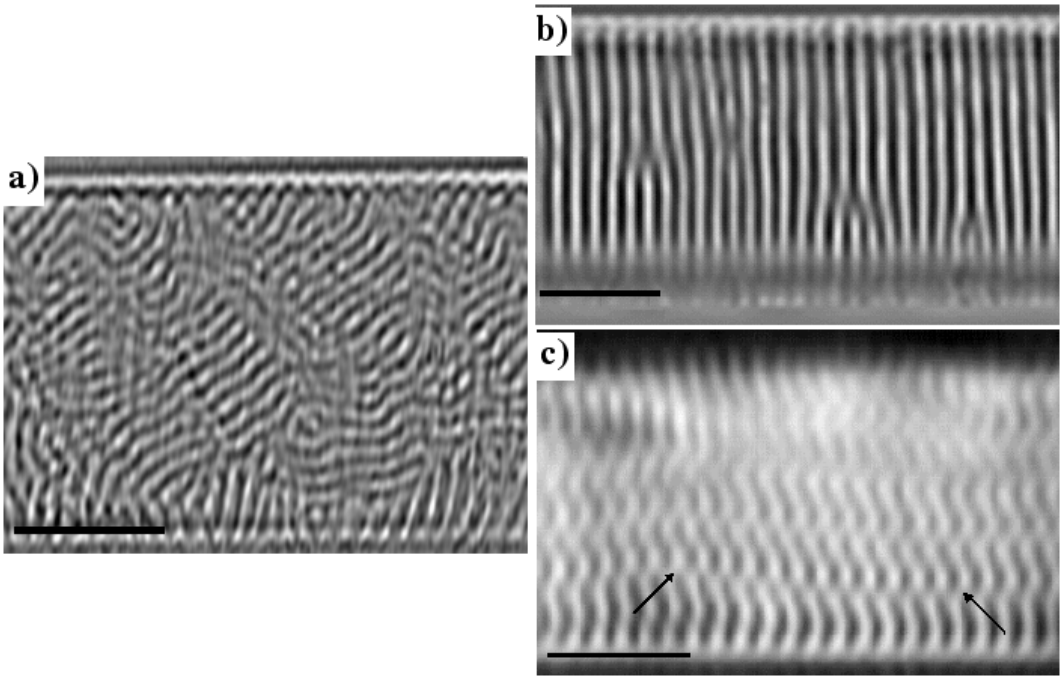

Figure 2: a) Disordered growth pattern 10 min after the onset of solidification at $V = 1\ \mu\text{ms}^{-1}$. b) Steady symmetrical pattern (with a few lamella terminations) and c) steady zigzag patterns (arrows: line defect) after 2 h of solidification at $V = 0.5\ \mu\text{ms}^{-1}$. Bars: 100 μm.

Phase Field Model and Simulation Setup

The phase-field model used here is based on the multi-phase-field approach [14]: the liquid L and the two solid phases α and β are described by three phase fields p_L, p_α and p_β which represent their local volume fractions. We use the model developed in Ref. [4] which has been extensively tested and calibrated in two dimensions against boundary integral simulations. The time evolution of the phase fields is given by

$$\tau(\vec{p})\frac{\partial p_i}{\partial t} = -\left.\frac{\delta \mathcal{F}}{\delta p_i}\right|_{\sum_i p_i = 1} \tag{1}$$

where $\vec{p}$ denotes the set of phase fields $\{p_\alpha, p_\beta, p_L\}$, $\tau(\vec{p})$ is a relaxation time, $\mathcal{F}$ is a free energy functional that depends on the values of the phase fields, their gradients, the temperature, and the composition c, and $\delta\mathcal{F}/\delta p_i$ denotes the functional derivative, which has to be taken subject to the constraint that the sum of all phase fields remains equal to one. The alloy composition c satisfies a conservation law,

$$\frac{\partial c}{\partial t} + \nabla \cdot \mathbf{J} = 0, \tag{2}$$

with the current given by

$$\mathbf{J} = -M(\vec{p})\vec{\nabla}\mu + \mathbf{J}_{\text{AT}}, \tag{3}$$

where μ is the chemical potential, $M(\vec{p})$ is a mobility which is taken to be zero in the solids in the one-sided model, and $\mathbf{J}_{\text{AT}}$ is the so-called antitrapping current which counteracts spurious solute trapping caused by the use of thick diffuse interfaces [3, 4].

All the details about the construction of the free energy functional $\mathcal{F}$ and the antitrapping current are given in Ref. [4]. An important point is that the model can accommodate arbitrary phase diagrams. Simulations were carried out for two alloy systems: a generic eutectic

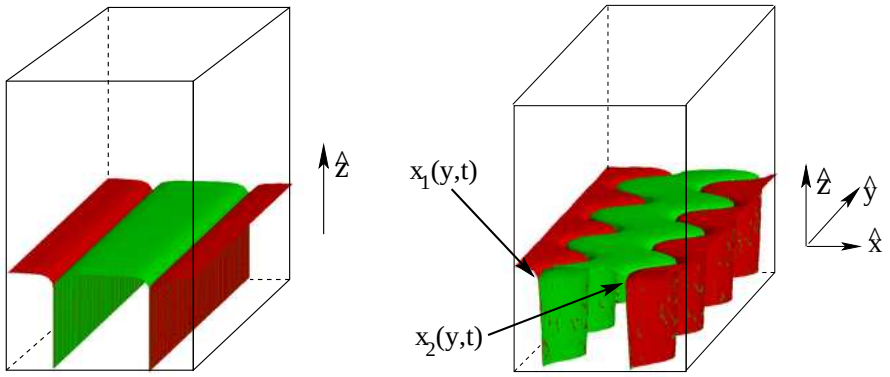

Figure 3: Illustration of the simulation geometry. Left: initial configuration. Growth is along z, lamellae are oriented along y. Right: an instability develops. The positions of the triple lines $x_i(y)$ are used to obtain its growth rate.

alloy with a completely symmetric phase diagram, and CBr_4-C_2Cl_6. As in the experiments, the temperature gradient was along z, and we started from straight lamellae aligned with the y direction, with no-flux boundary conditions at the ends. This corresponds to a regular initial state as depicted in Fig. 2b. The stability of lamellar arrays was investigated using simulations with a single lamella pair contained in a box with periodic or no-flux boundary conditions on the lateral sides; in the growth direction, the diffusion field was calculated on a hierarchy of several grids of different mesh size in order to fully resolve the solute boundary layer in a reasonable calculation time. The initial condition was a steady-state lamellar solution computed previously, supplemented by small random fluctuations of the phase-fields and the composition which trigger the instability.

Simulation Results

The straight lamellae can become unstable with respect to several different modes which break some of the multiple elements of symmetry contained in the unperturbed pattern, as shown in Fig. 4. There is a discrete translational symmetry along x and two planes of symmetry located at the centers of the two types of lamellae. When both symmetry planes survive, the pattern is still periodic with the same wavelength λ as the basic pattern; therefore, this instability will be referred to as 1-λ. In contrast, when one out of the two planes survives, the resulting pattern is periodic with a wavelength equal to twice λ; this instability will be called 2-λ. Finally, the instability which leads to a loss of both symmetry planes is known as the zigzag instability. By appropriately choosing the boundary conditions of the simulation box and following the triple line motion, the growth rates ω of these various instabilities can be extracted. For $\omega > 0$, an instability is active, whereas for $\omega < 0$, the perturbation decays and the system is stable.

A large number of such runs was carried out in order to determine the stability thresholds for different alloy compositions. The results for CBr_4-C_2Cl_6 are shown in the stability diagram, Fig. 5 (the results for the symmetric model alloy are qualitatively similar), and can be summarized as follows:

- Each of the instabilities described above is active for Λ larger than some critical value which depends on the type of the instability and on the alloy composition.
- The first instability to occur is always (for all compositions and alloy systems investigated) the zigzag instability.

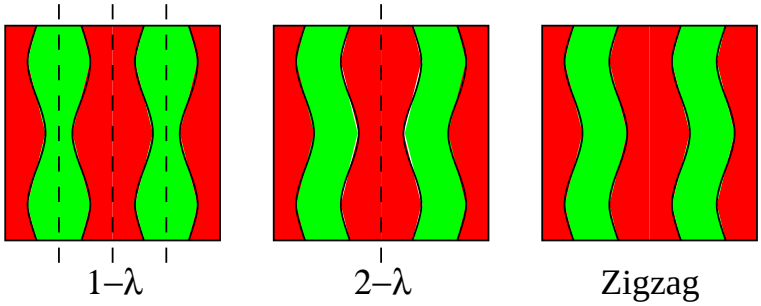

Figure 4: Various possible instabilities of straight lamellae.

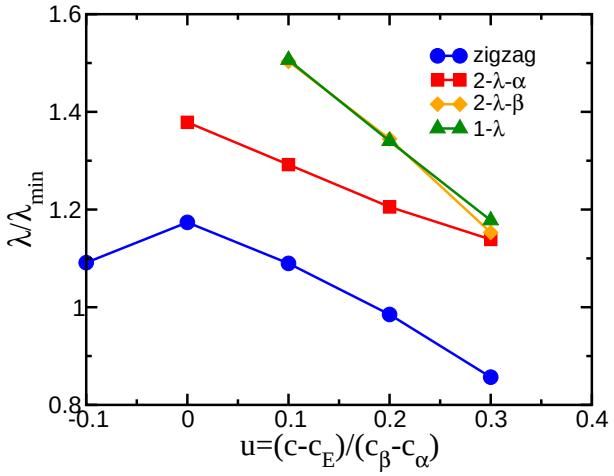

Figure 5: Stability diagram for CBr_4-C_2Cl_6 in the spacing-composition plane. The indicated modes are stable below the lines, and unstable above. $\lambda_{\min}$ is the Jackson-Hunt minimum undercooling spacing, and c_E, c_β and c_α are the compositions of the liquid and the two solids at the eutectic temperature.

- The zigzag instability is a long-wavelength diffusive instability, that is, the growth rate scales as $\omega = -D_\perp(\lambda)k^2$ for $k \to 0$, where k is the wave number along y (along the direction of the lamellae), and $D_\perp$ is a so-called phase-diffusion coefficient which changes sign at the critical spacing. As a consequence, the wavelength along y of the fastest growing mode strongly depends on λ.

- The other modes are finite-wavelength modes, that is, they occur with a well-defined wavelength along y that is almost independent of λ and comparable to λ. It can be shown that these modes are the three-dimensional extensions of the well-known oscillatory modes in two dimensions. Indeed, for k sufficiently small, ω becomes complex, which corresponds to oscillatory growth or decay.

- For small λ, the same lamella elimination instability as in two dimension occurs; no new instability was observed.

- The largest range of stable spacings occurs at the eutectic composition, as in two dimensions; however, the largest stable spacing is only about 1.2 $\lambda_{\min}$, whereas it is more than twice $\lambda_{\min}$ in two dimensions. This value seems to be quite robust: the simulations for the symmetric model alloy yield almost the same result.

The evolution of unstable lamellae beyond the linear instability regime was investigated by simulations in extended systems containing several lamellae pairs. Figure 6 shows such

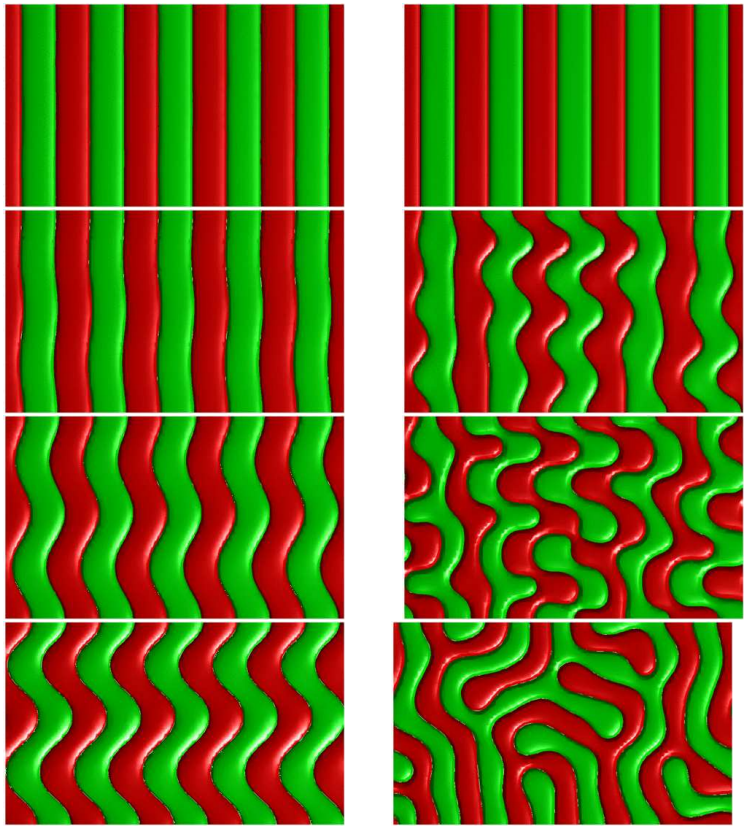

Figure 6: Evolution in extended systems. Left column: $\lambda/\lambda_{\min} = 1.3$. The final zigzag structure is stable. Right column: $\lambda/\lambda_{\min} = 1.6$. A labyrinth structure emerges, which continues to evolve on a very slow time scale until the end of the simulation.

simulations carried out for the symmetric model alloy at the eutectic composition, where the volume fractions of the two solid phases are equal. For λ closely above the instability threshold, a coherent zigzag pattern develops and saturates at a finite oscillation amplitude. For λ far from the threshold, several instabilities are active simultaneously, and the evolution of different lamellae is decoupled. Numerous pinching and reconnection events take place, and a labyrinth pattern develops which becomes more regular by the elimination of defects, but on a very slow time scale. Simulation times were not sufficient to reach a steady state.

Discussion

Clearly, the simulations are capable of reproducing the different patterns observed in the experiments, as can be seen by comparing Figs. 2 and 6. Both in simulations and experiments, lamellar patterns were found to destabilize and to form zigzag structures above a critical dimensionless spacing Λ_{zz}. The simulations show that the instabilities known from thin samples are still present, but are preceded by the zigzag instability for all alloy systems and compositions investigated.

The critical spacings Λ_{zz} determined from experiments and simulations slightly differ. This difference in too large to be attributed to uncertainties in the experimental control parameters or to numerical errors and must therefore be due to assumptions made in the model. Two possible causes are readily identified. First, for reasons of numerical efficiency detailed in Ref. [4], we have used in the simulations a somewhat smaller solid-solid surface tension than in the real alloy, which leads to different contact angles. Second, we have not included in the model any anisotropies of the surface tensions. In particular, anisotropy of

the solid-solid interfaces might play an important role in the stability of straight lamellar patterns. These issues will be clarified by future simulations.

The behavior of the disordered labyrinth patterns is complex and remains to be studied in detail, both in simulations and experiments. In the experiments, no patch of lamellae was ever observed to exhibit a spacing larger than $\Lambda = 1.1$. In the simulations, the reconnection and rearrangement of lamellae tends to reduce the large initial spacing toward a value closer to $\Lambda = 1$. This shows that, in three dimensions, there are many different mechanisms for spacing adjustment which need to be clarified.

This work was supported by Centre National d'Études Spatiales, France.

References

[1] A. Karma and W.-J. Rappel, "Quantitative phase-field modeling of dendritic growth in two and three dimensions", *Phys. Rev. E*, 57 (1998), 4323-4349.

[2] A. Karma, Y. H. Lee, and M. Plapp, "Three-dimensional dendrite tip morphology at low undercooling", *Phys. Rev. E*, 61 (2000), 3996-4006.

[3] B. Echebarria *et al.*, "Quantitative phase-field model of alloy solidification", *Phys. Rev. E*, 70 (2004), 061604.

[4] R. Folch and M. Plapp, "Quantitative phase-field modelling of two-phase growth", *Phys. Rev. E*, 72 (2005), 011602.

[5] C. Beckermann *et al.*, "Modeling melt convection in phase-field simulations of solidification", *J. Comput. Phys.*, 154 (1999), 468-496.

[6] J. C. Ramirez *et al.*, "Phase-field modeling of binary alloy solidification with coupled heat and solute diffusion", *Phys. Rev. E*, 69 (2004), 051607.

[7] K. A. Jackson and J. D. Hunt, "Lamellar and rod eutectic growth", *Trans. Metall. Soc. AIME*, 236 (1966), 1129.

[8] M. Ginibre, S. Akamatsu, and G. Faivre, "Experimental determination of the stability diagram of a lamellar eutectic growth front", *Phys. Rev. E*, 56 (1997), 780-796.

[9] A. Karma and A. Sarkissian, "Morphological instabilities of lamellar eutectics", *Metall. Mat. Trans. A*, 27 (1996), 635-656.

[10] S. Akamatsu *et al.*, "Overstability of lamellar eutectic growth below the minimum-undercooling spacing", *Met. Mat. Trans A*, 35 (2004), 1815-1828.

[11] S. Akamatsu, S. Bottin-Rousseau, and G. Faivre, "Experimental evidence for a zigzag bifurcation in bulk lamellar eutectic growth", *Phys. Rev. Lett.*, 93 (2004), 175701.

[12] S. Akamatsu, S. Moulinet, and G. Faivre, "The formation of lamellar eutectic grains in thin samples", *Met. Mat. Trans A*, 32 (2001), 2039-2048.

[13] P. Manneville, *Dissipative structures and weak turbulence*, (Boston, MA: Academic Press, 1990).

[14] I. Steinbach *et al.*, "A phase field concept for multiphase systems", *Physica D*, 94 (1996), 135-147.